CARBOXYLATED GRAPHENE-TiO2 HYBRIDS AS MULTIFUNCTIONAL MATERIALS: FROM PHOTOCATALYSIS TO PEROXIDASE ALTERNATIVES

CARBOXYLATED GRAPHENE-TiO_2 HYBRIDS AS MULTIFUNCTIONAL MATERIALS: FROM PHOTOCATALYSIS TO PEROXIDASE ALTERNATIVES.

M. Sarro [(1)], M. Cerruti [(2)], P. Calza* [(1)], L. Anfossi [(1)]

(1) Università di Torino, Dipartimento di Chimica, via P. Giuria 5- 10125 Torino- Italy

(2) McGill University, Materials Engineering, Montreal, Canada

*corresponding author: e-mail: paola.calza@unito.it; phone +390116705268; fax: +390116705242

Abstract

We synthetized hybrid materials with multifunctional properties by coupling graphene nanoplatelets (GNP) modified with carboxylic groups to titanium dioxide (TiO_2) nanoparticles (NPs) and tested them both as photocatalysts to promote pollutant abatement and as tracers of the presence of a model antigen (bovine serum albumin, BSA) in immunochemical assays. The presence of carboxylic groups proved to be crucial in both applications: they improved TiO_2 photocatalytic activity by the interaction between the carboxylic groups on the GNP surface and the hydroxyl groups on TiO_2 surface, and allowed for covalently binding the material to BSA. The photoactivity of the materials was exploited for the oxidation of 3,3',5,5'-tetramethylbenzidine for immunochemical applications.

Keywords: functionalized graphene, immunoassay, TiO_2, photodegradation

1. Introduction

Titanium dioxide is one of the most widespread used photocatalyst because of its low cost, high chemical stability, non-toxicity and photostability; still, its efficiency is limited by the fast recombination of the generated electron-hole pairs[1,2]. Many researchers have tried to improve TiO_2 photocatalytic activity[3,4,5] with strategies including surface modification with metal particles[6,7], semiconductor coupling[8,9], or using carbon nanoparticles (CNPs)[10,11,12,13]. More recently, graphene was suggested as a material able to enhance TiO_2 photocatalytic efficiency by hindering the charge recombination process[14,15,16,17] thanks to its high charge carrier mobility[18,19].

The phase, size, shape and extent to which different TiO_2 facets are developed govern TiO_2 activity as well[20,21]. Previously, we used functionalized graphene nanoplatelets (GNP) as a substrate to control phase, shape and exposed facets of TiO_2 NPs in GNP-TiO_2 nanocomposites[22]. We showed that both aminated and carboxylated GNP (NH_2-GNP and COOH-GNP, respectively) were able to change the morphology of TiO_2 nanoparticles (NPs) grown during hydrothermal synthesis, and we reported for the first time TiO_2 NPs resting on graphene sheets with the most reducing {101} facets. This hybrid material showed more efficient phenol photodegradation compared to both TiO_2 NPs alone and other hybrid materials where the TiO_2-GNP coupling was not controlled[23].

We proposed using TiO_2 NPs in a different application, i.e., as a substitute for horseradish peroxidase (HRP) to catalyze H_2O_2 dismutation in immunochemical assays. Immunoassays are based on a specific antigen-antibody reaction and use enzymes such as HRP as catalysts to amplify the signal produced during H_2O_2 dismutation upon oxidation of a chromogenic substrate (e.g., 3,3',5,5'-tetramethylbenzidine, TMB). This principle is at the basis of the most common biosensing assays, such as the determination of glucose or cholesterol; and similar immunoassays are widely used in clinical, environmental and food analysis due to their sensitivity, selectivity, versatility and simplicity[24]. However, natural enzymes such as HRP have intrinsic drawbacks: they can be easily denatured by environmental changes (e.g. pH and temperature); and they are difficult and expensive to prepare and purify. Inorganic nanoparticles are a suitable alternative to natural enzymes thanks to their low-cost synthesis, high stability and versatility[25]. Already several researchers attempted using inorganic nanoparticles as a substitute for enzymes in biosensing and immunoassays, for example metal oxides (i.e. Fe_3O_4[26] and Co_2O_3[27]), Pt nanoparticles[28], and graphene oxide[29].

Here we synthesize functionalized GNP-TiO_2 NPs hybrids that show both enhanced photocatalytic activity toward the abatement of pollutants and as HRP alternatives in immunochemical applications. We synthetized the GNP-TiO_2 hybrids following a procedure based on our previous work[20]: we used the most active COOH-GNP substrate, and we changed the Ti^{4+} complexing agent from triethanolamine to acetic acid. This caused a change in solution pH, which we expected to cause different shape of TiO_2 NPs because of the change of pH[30]. The presence of carboxylic functionalities on GNP allowed us to couple the GNP flakes not only to the TiO_2 NPs, but also to the immunoreactants used in a typical immunoassay. Our results showed that the presence of GNP-COOH in the composite leads to an improvement of the photoactivity of the TiO_2 and we exploited this property for possible application of the novel composite material as a signal generating probe in immunochemical methods of analysis. For this study, we prepared a hybrid material by binding bovine serum albumin (BSA) to the composite GNP-TiO_2-COOH, through linking –COOH groups with the protein and evaluated the peroxidase-mimicking ability of the hybrid material, thus introducing GNP-TiO_2 composite as multifunctional materials for both environmental and immunoassay applications.

2. Materials and methods

2.1 GNP functionalization

GNP (Graphene Supermarket, 3 nm flakes, Grade AO1, lateral size 10 µm) was modified with carboxylic groups using diazonium chemistry, as described by Sordello et al.[22]. Briefly, GNP was added to a 0.5 M HCl solution containing 0.05 M 4-aminophenylacetic acid (4-APA) reaching a final GNP concentration of 1 mg/ml. The reaction was carried out for 10 minutes under vigorous stirring. During this time, 4-APA was reduced to diazonium cations and then radicals in the presence of GNP, and these reacted with GNP creating COOH groups on its surface (Fig. S1).[22] The functionalized GNP was then filtered and washed five times with isopropanol and five times with deionized water, and allowed to dry overnight at room temperature. The resulting material, denoted GNP-COOH, was characterized via X-ray Photoelectron Spectroscopy (XPS), IR and Raman (Figs. S2-S4), thus confirming effective functionalization.[22]

2.2 Composite material synthesis

TiO_2-GNP composite materials were synthesized using a hydrothermal method similar to that described in Sordello at al.[22], but using acetic acid instead of triethanolamine. 5 ml of the TiO_2 precursor titanium isopropoxide (TIP) were mixed with 10 ml of glacial acetic acid under vigorous stirring for 30 minutes. After this, the solution volume was brought to 50 ml by adding deionized water. This constituted the stock solution. Either 5 mg or 1 mg of GNP or GNP-COOH were added to 10 ml of stock solution to synthetize hybrid materials with different amounts of GNP or functionalized GNP and the final volume was brought up to 60 ml with deionized water. The pH of the solutions was around 2.4-2.5 in all samples. The solution was put into a Teflon autoclave and TiO_2 nucleation and growth occurred while heating the reaction vessel at 383 K for 24 h, and then at 418 K for 72h[20]. We denote the resulting materials as GNP-TiO_2-08, GNP-TiO_2-3, GNP-COOH-TiO_2-08, and GNP-COOH-TiO_2-3, where the number after TiO_2 refers to the weight % of GNP measured by TGA (vide infra). We also synthesized TiO_2 NPs in the absence of GNP using the same procedure. The solution pH was again 2.4-2.5. A summary of all samples analyzed in this work is presented in Table S1.

2.3 Material characterization

XPS spectra were measured on a monochromatic X-ray photoelectron spectrometer K Alpha (Thermo Scientific) equipped with an Al Ka X-ray source (1486.6 eV, 0.834 nm), a microfocused monochromator, and an ultrahigh vacuum chamber (10^{-9} Torr). Survey scans (five points for each sample) and high resolution scans (three points for each sample) were collected with energy steps of 1 and 0.1 eV, respectively, using an X-ray beam spot 400 µm wide. The spectral energies were calibrated by setting the binding energy (BE) of the C_{1s} component corresponding to C–C bonds to 284.4 eV.

Raman spectra were taken with a Bruker Senterra Raman Microscope using a 785 nm laser and a 40X objective. At least eight points were analyzed on each sample.

Thermogravimetric analysis (TGA) was performed using a Q500 instrument from TA instruments. Analyses were performed in air, with a heating rate of 20 K min^{-1}, and Pt pans were used as sample holders.

Transmission electron microscopy (TEM) images were taken on a Philips CM200 instrument operating at up to 200 kV, with line resolution of 0.14 nm and point resolution of 0.19 nm.

2.4 Photocatalytic test

Orange II was chosen as model molecule to investigate the photocatalytic efficiency of the synthesized materials. 5 mL of an aqueous solution containing orange II (10 mg L^{-1}) and the catalyst (0.5 g L^{-1}) were placed in Pyrex glass cells. Solutions were kept under magnetic stirring and irradiated using a TL K05 UV/A lamp with 25 mW m^{-2} power and maximum emission at 365 nm. Since these composite materials are intended for environmental applications, we evaluated if once dispersed in aqueous solution they can be efficiently removed at the end of the treatment. After illumination, the entire content of each cell was filtered through a 0.45 µm Millipore filter in order to eliminate the catalyst. The UV-Vis spectra and TOC analysis performed on filtered solutions permit to assess the efficient catalysts removal. The disappearance of orange II in solution was followed as a function of irradiation time via UV-vis spectroscopy, using a Varian CARY 100 Scan UV–vis spectrophotometer and Suprasil quartz cuvettes with a path length of 1 cm. The spectrophotometric determination was done at 486 nm.

2.5 Labelling of bovine serum albumin (BSA) with GNP-COOH-TiO_2

Conjugation with BSA was achieved by mixing 1 ml of a suspension of both composites GNP-COOH-TiO_2 (1 mg/ml) with 50 µl of EDAC (10 mg/ml) for 20 minutes, in order to activate the carboxylic groups on GNP surface. Then, 0.5 ml of the BSA solution (10 mg/ml) were added and the resulting solution was stirred for 30 minutes. After this, another 50 µl of EDAC were added to the solution and the reaction was carried out for 24 hours[31]. All the solutions were prepared in phosphate buffer 20 mM (pH 7.4). The obtained material, denoted GNP-COOH-TiO_2-BSA, was collected by centrifugation and washed 4 times with deionized water to eliminate excess BSA. Successful conjugation of the protein to the composite material was qualitatively confirmed by staining with the Brilliant Blue Comassie reagent.

2.6 Catalytic activity of the immunochemical probe

The experimental conditions were optimized by investigating the best ratio between TMB and H_2O_2, in order to obtain the highest useful signal for the analysis; and by studying the kinetic of oxidation of orange II between 10 minutes and 2 hours. Irradiation experiments were carried out in uncoated microplates filled with 100 µl of the GNP-COOH-TiO_2-BSA solution (1 mg/l) and 100 µl of TMB mixed with H_2O_2. All chemicals were prepared in MilliQ water. Samples were irradiated using a 40 Watt Philips TLK/05 lamp with maximum emission at 360 nm. After the addition of 50 µl of H_2SO_4 2 M (stop solution), TMB absorbance was recorded at 450 nm by means of a microplate reader (Multiskan FC, Thermo Fisher Scientific).

2.7 Stability of the materials

GNP-COOH-TiO_2-BSA long-term stability was studied by diluting the NPs (1 mg/l) in phosphate buffer solutions at room temperature for 14 days or at 50°C for 1 hour, and at pH values ranging from 2 to 10 for periods of 1, 4 and 24 hours. Similar experiments were carried out at different saline concentrations (0.15 M and 0.5 M NaCl), to mimic different ionic strengths of biological fluids.

2.8 Activity test after immune-complex formation

The ability of the conjugated hybrid material to act as a label for immunoassay was tested by measuring the oxidizing capacity of GNP-COOH-TiO_2-BSA bound to anti-BSA antibodies coated onto the surface of microtitre wells. To coat the wells, anti-BSA rabbit polyclonal antibodies (Sigma-Aldrich) were diluted 1:10000 in carbonate/bicarbonate buffer (pH 9.6) and 150 µl were left in contact with the surface of microtitre wells overnight at 4°C. The wells were then washed

three times with 300 µl of 0.05% (v/v) Tween 20 (washing protocol) to remove unbound antibodies. Unless specified, the same washing procedure was applied from here on out. To ensure complete saturation of the well surface, we added 250 µl of phosphate buffer containing 1% (w/v) casein; we allowed the solution to stay in the wells for 1 hour at room temperature, and then washed them.

GNP-COOH-TiO_2-BSA NP solutions prepared in phosphate buffer at concentrations of 0.4, 1, 4 and 10 µg/ml were left in contact with the coated wells for 24 h, after which any unbound NP was removed by washing. The catalytic activity of the bound fraction of GNP-COOH-TiO_2-BSA was measured as detailed in section 2.6 by adding the optimal TMB/H_2O_2 mixture under UV irradiation for one hour.

3. Results

3.1 Synthesis and characterization of composite materials

We synthesized both pristine TiO_2 and the hybrid materials following the same procedure described in [20], but we used acetic acid instead of triethanolamine as complexing agent for the Ti^{4+} ions.

Raman spectroscopy showed that the crystalline phase of TiO_2 nanoparticles was anatase, as indicated by the presence of only the peaks below. In particular, the five well-resolved peaks at 144 cm^{-1} (Eg), 197 cm^{-1} (Eg), 395 cm^{-1} (B1g), 513 cm^{-1} (B1g + A1g) and 634 cm^{-1} (Eg) are the characteristic vibrations of anatase (Fig. 1).

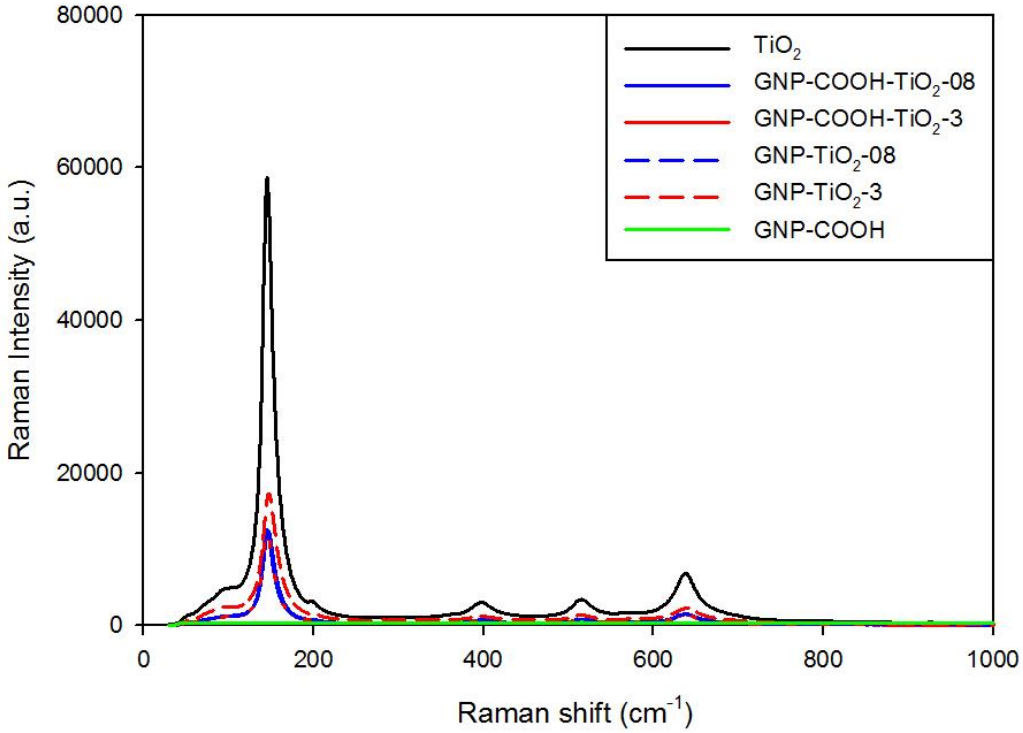

Figure 1: Raman spectrum of pristine TiO_2 and hybrid materials in the 0-1000 cm^{-1}

We estimated the amount of graphene present in the samples by TGA (Fig. 2). The weight loss occurring at 350–400 K on the hybrid samples can be attributed to dehydration. At 600 K, the overall weight loss for the hybrid samples goes from 0.8 % to 3 %. At this temperature we had a weight loss of the pure GNP sample of about 100% (see Figure S5), so the amount of GNP in our

samples goes from 0.8% to 3%. Consequently we denote the samples as GNP-COOH-TiO_2-3, GNP-COOH-TiO_2-0.8, GNP-TiO_2-3 and GNP-TiO_2-0.8.

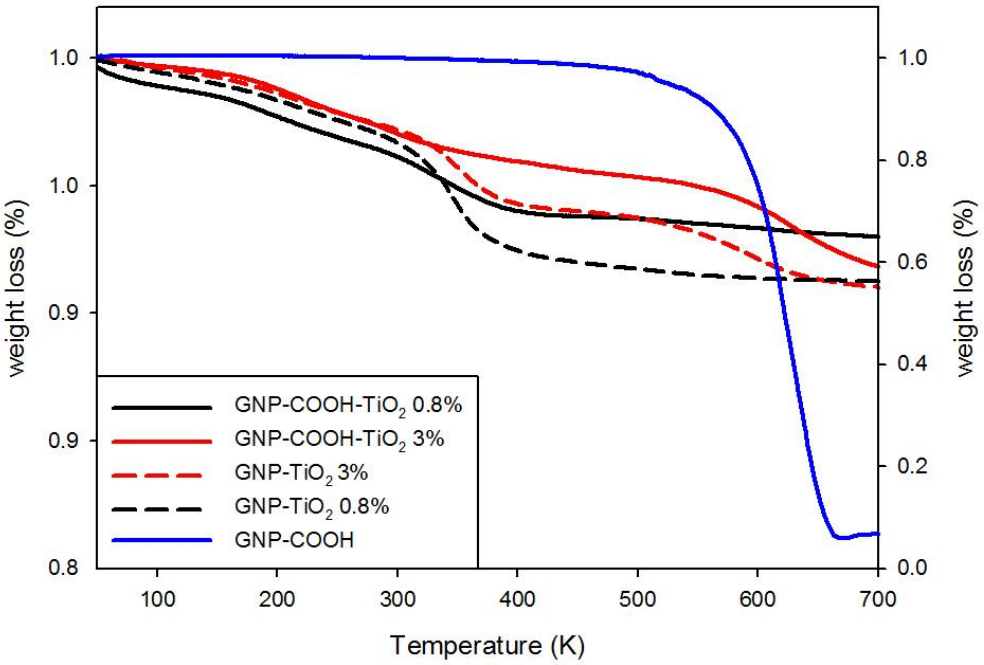

Figure 2: Normalized weight (%) as a function of the temperature; right y-axis refers to GNP-COOH.

TEM micrographs were recorded for TiO_2 NPs and composite materials and are shown in Fig. 3. The low magnification images show well dispersed particles in all samples, with shapes that include mostly truncated bipyramids or cuboids, and occasional ellipsoids. GNP-TiO_2 (Figs. 3C-D) and GNP-COOH-TiO_2 (Figs 3E-F) hybrids show TiO_2 NPs well dispersed on GNP sheets, with dimensions (10-15 nm by 7-10 nm) and shapes similar to those observed for TiO_2 NPS alone (Figs. 3A-B). This result implies that the addition of graphene did not strongly influence NP nucleation and growth; this is different from what we found in our previous work[22], where we showed control over NP shape in the presence of GNP-COOH. This difference can be explained by the fact that here we have used acetic acid as Ti^{4+} complexing agent, which implies that the synthesis of all materials (TiO_2 NPs and hybrids) was carried out at a pH of 2.3-2.4. In our previous work, we had attributed the difference in the shape of the NP synthesized on GNP-COOH to differences in local pH due to the presence of surface carboxylic groups; here, the already acidic bulk pH does not allow the acidic surface functionalities to exert a specific effect on NP morphology.

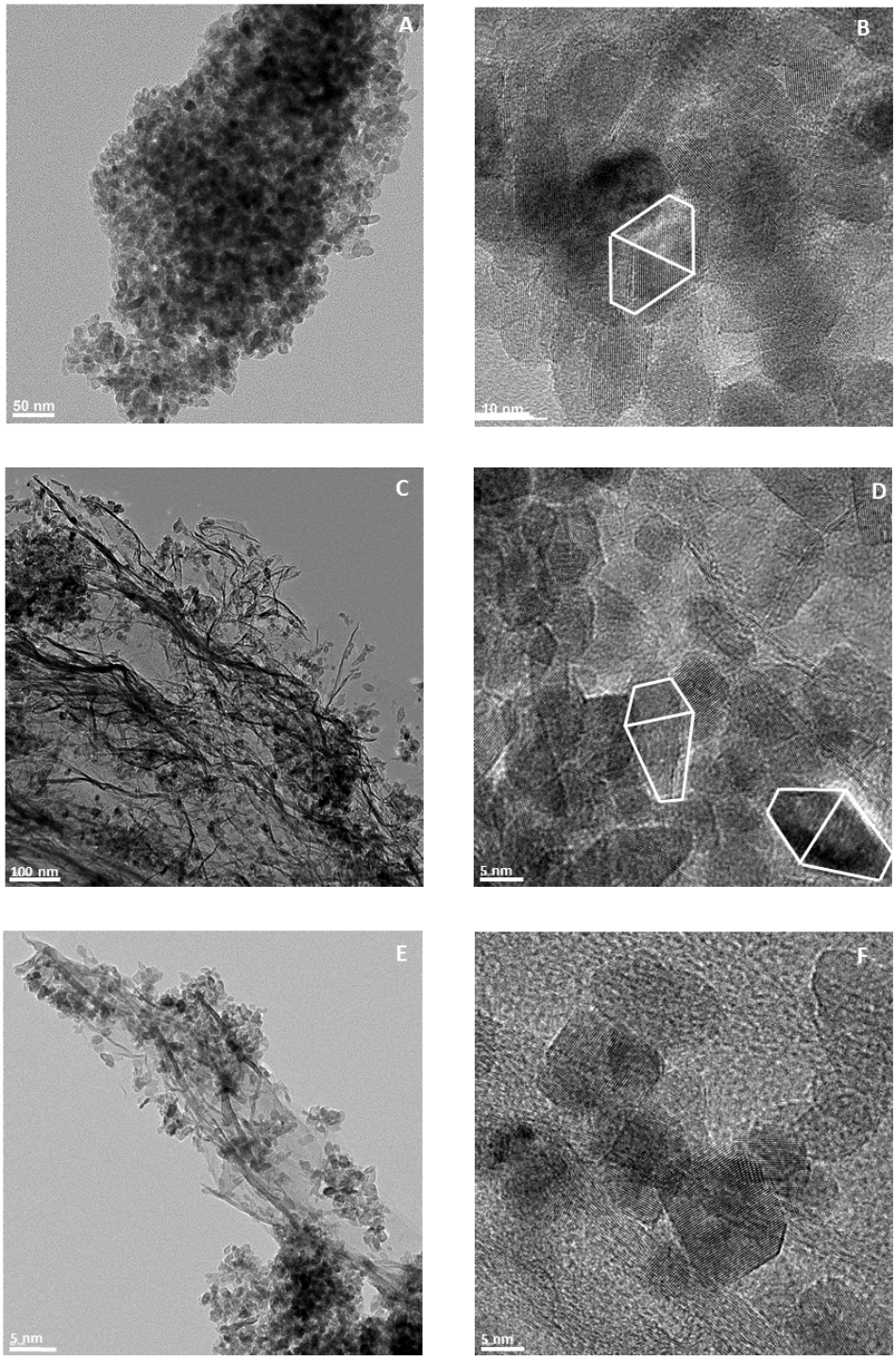

Figure 3. TEM micrographs for pristine TiO_2 at low resolution (A) and high resolution (B); GNP-TiO_2 at low resolution (C) and high resolution (D); and GNP-COOH-TiO_2 at low resolution (E) and high resolution (F)

3.2 Photocatalytic activity

We studied the photocatalytic activity of the hybrid materials and of TiO_2 NPs using orange II as a model compound. At first we evaluated the extent of dye adsorption on all materials by performing experiments in the dark (Fig. 4A). After one hour of contact, the adsorption is negligible on TiO_2 NPs, while almost 20% of dye was adsorbed on GNP-TiO_2-08, and 50% on GNP-TiO_2-3. This can be attributed to dye adsorption on graphene through Van der Waals forces[32]. Dye adsorption is reduced to 3 and 18%, respectively, on the hybrid materials obtained using functionalized gra-

phene (GNP-COOH-TiO_2-08 and GNP-COOH-TiO_2-3). This is probably due to the negatively charged –COOH groups, which electrostatically repelled orange II, an anionic dye negatively charged at the pH investigated (pH=5.4).

The disappearance curves for orange II as a function of irradiation time are shown in Fig. 4B. TiO_2 and GNP-TiO_2 hybrids promote a similar dye degradation, with phenol half time life of 35 min. By comparing the disappearance curves, it can be noted a slight increase for GNP-TiO_2-3 at short irradiation times, which could be ascribed to the adsorption contribution described above rather than to an increased photoactivity of the composite material. Conversely, the dye abatement is faster in the presence of GNP-COOH-TiO_2 hybrids. In particular, GNP-COOH-TiO_2-3 exhibits the best photocatalytic performance, with phenol half time life of 20 min. These results could be ascribed to both dye adsorption (Fig. 4A) and enhanced photocatalytic activity. The increased photoactivity may be explained by the strong interactions between the hydroxyl groups present on the surface of TiO_2 NPs and the carboxylated groups on GNP-COOH, which favor charge transfer from TiO_2 to GNP [33] and could effectively inhibit electron–hole recombination. Stability of the materials was checked as well and, after three cycles, the photoactivity is maintained (Fig. S6).

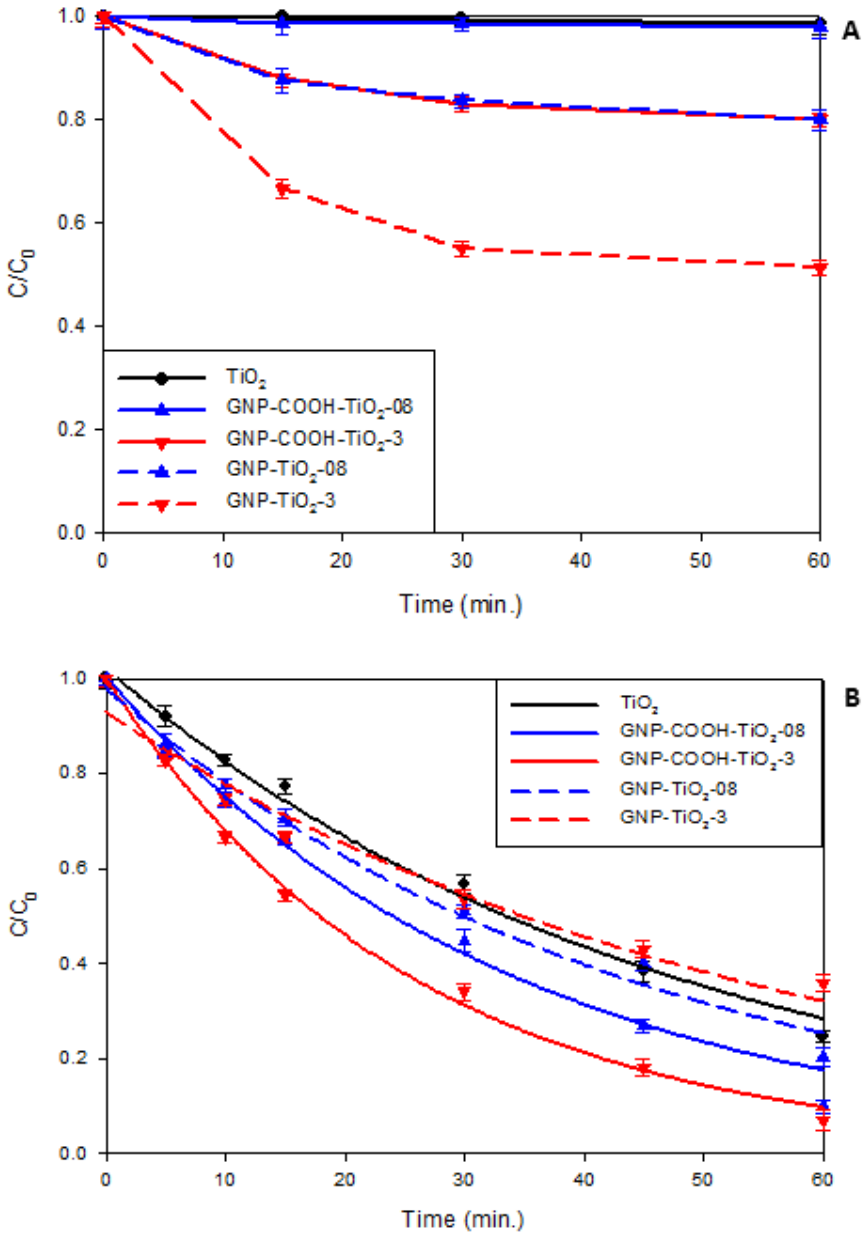

Figure 4: Orange II degradation as a function of time in the dark (A) and under UV A light (B).

3.3. HRP-like activity

After proving that the composite materials are photoactive, we tested them as alternatives to HRP to oxidize TMB. We focused on the GNP-COOH-TiO_2 samples, since they were the most active materials, and recorded the change in color related to TMB oxidation in the presence of the NPs and various amounts of H_2O_2, ranging from no H_2O_2 to 6 times as much H_2O_2 as TMB. The absorbance values reported are the difference between the overall signals and the signals due to self-oxidation of TMB under UV irradiation and to the non-specific binding of the NPs on the walls of the microplates. Results show that the oxidation of TMB is strongly dependent on the amount of H_2O_2 (Fig. 5); this proves the HRP-like activity of the materials[30]. The largest signals are obtained using the highest amount of H_2O_2 and GNP-COOH-TiO_2-08. Conversely in the photocatalytic test with orange II the best performing material was GNP-COOH-TiO_2-3. This could be attributed to the

effect of the material on the adsorption of the dye that leads to a stronger interaction with the materials, while we do not expect H_2O_2 to be adsorbed on the materials. The signal observed by the optimal combination of TMB/H_2O_2 and GNP-COOH-TiO_2-08 is sufficiently intense to conceive the exploitation of this hybrid material as a probe for immunoassay, alternative to the enzymatic probe.

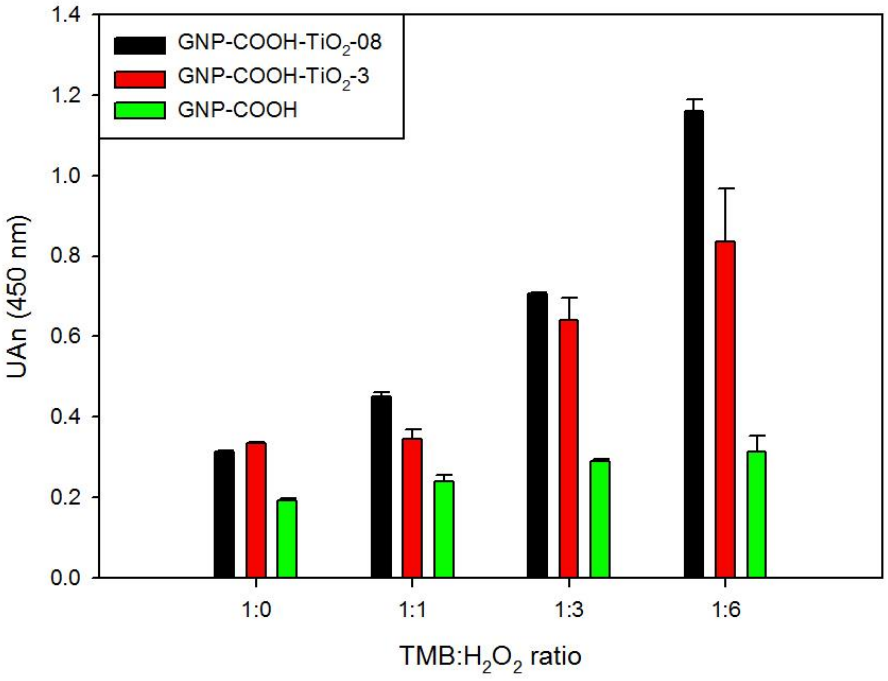

Figure 5: UA (Absorbance Units) measured at 450 nm indicative of TMB oxidation in the presence of GNP-COOH-TiO_2-08 and GNP-COOH-TiO_2-3 NPs as a function of TMB:H_2O_2 ratio. All measurements were repeated 3 times.

3.5 Stability of the hybrid material at different pH, temperature and saline concentration.

We investigated the stability of the GNP-COOH-TiO_2-08 material in conditions that inhibit the catalytic activity of natural enzymes. We chose to investigate the stability of this material because it is the most active between the two. We worked with a ratio TMB:H_2O_2 of 1:6, which leads to a higher signal. Contrary to HRP, the NPs are stable and preserve their catalytic activity at both low and high pH (Fig. 6A) and at different NaCl concentrations (Fig. 6B). Moreover after leaving GNP-COOH-TiO_2-08 for 12 days at room temperature we obtained a constant signal (Fig. 6C).

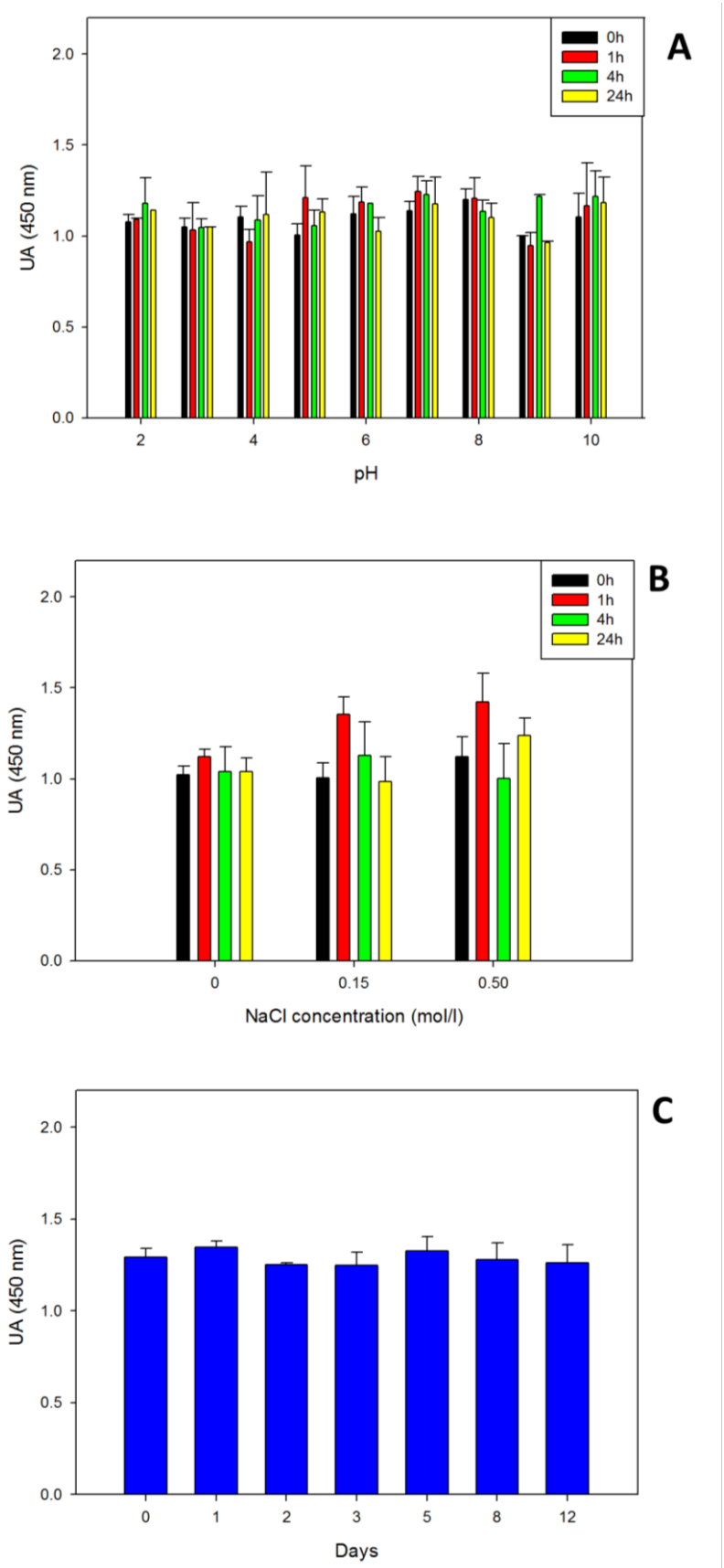

Figure 6: UA (Absorbance Units) measured at 450 nm indicative of TMB oxidation in the presence of GNP-COOH-TiO_2-08 NPs using a TMB:H_2O_2 ratio of 1:6 after 1, 4 and 24 h at different pH (A) and NaCl different concentration (0M, 0.15M and 0.50M) at pH 7 (B), and in PBS buffer 20 mM at pH=7.4 for up to 12 days (C). All measurements were repeated 3 times.

3.6 Activity of the hybrid materials after immuno-complex formation

To test the application of the hybrid materials in real immunological assays, we bound BSA on GNP-COOH-TiO_2-08 by covalently coupling the carboxylate groups present on GNP-COOH to the amino groups present on BSA (see section 2.5 for details). We then placed the resulting GNP-COOH-TiO_2-08-BSA NPs in contact for 24 h with microplate wells coated with anti-BSA antibodies. After removing unbound probes by washings, we measured the oxidation of TMB in the presence of H_2O_2 using a TMB:H_2O_2 ratio of 1:6. The experiment was repeated with increasingly diluted NP solutions, down to a concentration of 0.04 μg/ml, to test the sensitivity of the assay.

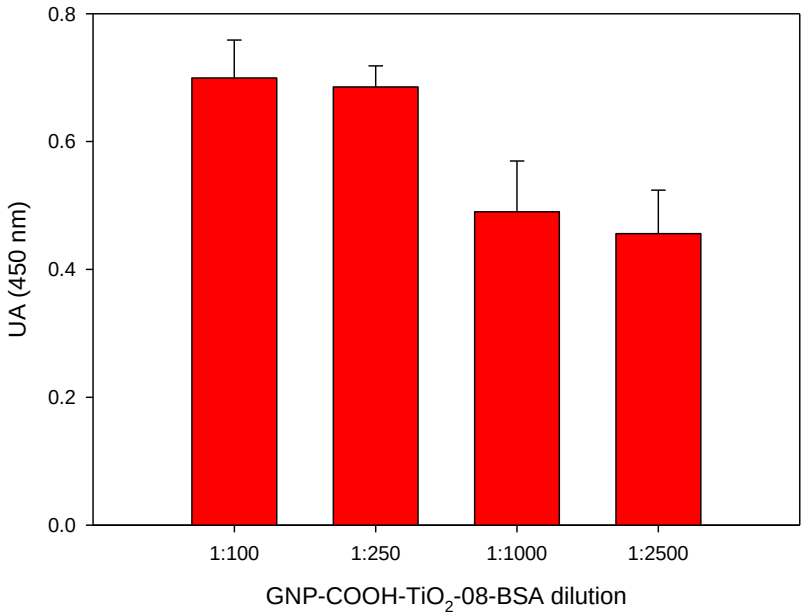

Figure 7: UA (Absorbance Units) measured at 450 nm, which relates to the oxidation of TMB by GNP-COOH-TiO_2-BSA after formation of the immunocomplex with immobilized anti-BSA. The values reported are the difference between the absorbance measured on the samples and that due to non-specifically bound probes and TMB self-oxidation. The experiments were performed at different GNP-COOH-TiO_2 dilutions, starting from an initial concentration of 0.1 mg/ml. All measurements were repeated 3 times.

TMB oxidation was detected at all NP dilutions, which indicates that the intrinsic HRP-like activity of GNP-COOH-TiO_2 NPs can still be detected after covalently linking to BSA, and that BSA is still intact and accessible enough after conjugation to GNP-COOH-TiO_2 to allow for selective recognition and binding onto anti-BSA antibodies. Lowering the initial concentration of GNP-COOH-TiO_2-BSA caused a decrease in signal measured. Since the signals reported do not include aspecific binding and TMB auto-oxidation, this result indirectly proves the formation of a specific bond between GNP-COOH-TiO_2-BSA and the immobilized antibodies.

4. Conclusions

We synthesized hybrid materials coupling functionalized GNP and TiO_2 NPs with the goal of achieving a versatile platform that could be used both for the abatement of contaminants and for immunochemical application. For both purposes, we exploited the presence of –COOH groups on GNP. In the case of contaminant abatement, modeled using Orange II dye, the presence of these functional groups led to an increase of the photocatalytic activity compared to both TiO_2 NPs and TiO_2 NPs coupled with unmodified GNP, likely due to the stronger interaction achieved between the carboxylated GNP and the hydroxyl groups present on TiO_2 NPs. In the immunochemical

application studied, we exploited the -COOH groups both for the improvement of the photocatalytic activity of the materials and because it allowed for the direct conjugation of BSA as model protein to the GNP-COOH-TiO_2 NPs. The resulting materials maintained HRP-like activity both before and after formation of the immunocomplex with immobilized anti-BSA and were stable in harsh conditions where natural enzymes such as HRP would be denatured.

Acknowledgments

We acknowledge support from a Marie Curie International Research Staff Exchange Scheme Fellowship (PHOTOMAT, proposal no. 318899) within the 7th European Community Framework Programme and from the Canada Research Chair program.

References

1. D. R. Hoffmann, S. T. Martin, W. Choi and D.W. Bahnemann *Chem. Rev,* 1995, **95***,* 69-96.
2. P.Muthirulan, C.NirmalaDevi and M.Meenakshi Sundaram, *Mater. Sci. Sem-icond. Process.,* 2014, **25**, 219-230.
3. H. Wang, T. You, W. Shi, J. Li and L. Guo *J. Phys. Chem. C,* 2012**, 116**, 6490-6494.
4. S. Hoang, S.P. Berglund, N.T. Hahan, A.J. Bard and C.B. Mullins *J. Am. Chem. Soc*., 2012, **134**, 3659-3662.
5. H. Kim, J. Kim and W. Choi *J. Phys. Chem. C*, 2011, **115**, 9797-9805.
6. G.M. Veith, A.R. Lupini and N.J. Dudney, *Phys. Chem. C* , 2009, **113**, 269-280.
7. J.C. Yu, G. Li, X. Wang, X. Hu, C.W. Leung and Z. Zhang, *Chem. Commun*., 2006, **25**, 2717-2719.
8. J.R. Raji and K. Palamivelu, *Ind. Eng. Chem. Res,.* 2011, **50**, 3130-3138.
9. W. Han, P. Liu, R. Yuan, J. Wang, Z. Li, J. Zhuang and X. Fu, *J. Mat. Chem.,* 2009, **19**, 6888-6895.
10. Y.J. Xu, Y. Zhuang and X. Fu, *J. Phys. Chem. C* 2010, **114,** 2669-2676.
11. B. Qiu, M. Xing, J. Zhang, *J. Am. Chem. Soc*. 2014, **136**, 5852−5855
12. F. Zhang, X. Carrier, J.M. Krafft, Y. Yoshimura and J. Blanchard, *New J. Chem*., 2010, **34**, 508-513.
13. B. Qiu, M. Xing, Q. Yi, J. Zhang, , *Angew. Chem*. 2015, **127**, 10789–10793
14. Q. Xiang, J. Yu and M. Jaroniec, *J. AM. Chem. Soc*., 2012, **134**, 6575-6578.
15. H. Zhang, X. Lu, Y. Li and J. Wang, *ACS Nano,* 2011, **5**, 590-596.
16. K. Li, J. Xiong, T. Chen, L. Yan, Y. Dai, D. Song, Y. Lu and Z Zeng, *J. Hazard. Mat*. 2013, **250**, 19-28.
17. K. Li, T. Chen, L. Yan, Y. Dai, Z. Huang, J. Xiong, D. Song, Y. Lu and Z. Zeng, *Colloid. Surf. Physic. Engineer. Aspc*., 2013, **422**, 90-96.
18. O. Akhavan and E. Ghaderi, *J. Phys. Chem. C,* 2009, **113**, 20214-20220.
19. H. Wang, T. Maiyalagan and X. Wang, *ACS Catal.,* 2012, **2**, 781-794.
20. U. Diebold, *Surf. Sci. Rep.,* 2003, **48**, 53-229.
21. T. Taguchi, Y. Saito, K. Sarukawa, T. Ohno and M. Matsumura, *New J. Chem.,* 2003, **27**, 1304-1306.
22. F. Sordello, G. Zeb, K. Hu, P. Calza, C.Minero, T. Szkopek and M. Cerruti, *Nanoscale,* 2014, **6**, 6710-6719.
23. F. Sordello, E. Odorici, K. Hu, C.Minero, M. Cerruti and P. Calza *Nanoscale,* 2016, **8***,* 3407-3415.
24. J. Mu, Yan Wang, M. Zhao and L. Zhang *Chem. Commun.,* 2012, **48**, 2540–2542.
25. L. Hu, Y. Yuan, L. Zhang, J. Zhao, S. Majeed and G. Xu, *Anal. Chim. Acta,* 2013, **762**, 83– 86.
26. L. Gao, J. Zhuang, L. Nie, J. Zhang, Y. Zhang, N. Gu, T. Wang, J. Feng, D. Yang, S. Perrett and X. Yan, *Nature Nanotec.,* 2007, **2**, 577-583.
27. J. Mu, Y. Wang, M. Zhao and L. Zhang, *Chem. Commun.,* 2012, **48**, 2540–2542.
28. K. Cai, Z. Lv, K. Chen, L. Huang, J. Wang, F. Shao, Y. Wang and H. Han, *Chem. Commun.,* 2013, **49**, 6024-6026.
29. Y. Song, K. Qu, C. Zhao, J. Ren and X. Qu, *Adv. Mater.,* 2010, **22**, 2206–2210.
30. A. S. Barnard and L. A. Curtiss, *Nano Lett.* 2005, **5**, 1261–1266.

31. L. Anfossi, P. Calza, F. Sordello, C. Giovannoli, F. Di Nardo, C. Passini, M. Cerruti, IY. Goryacheva, ES. Speranskaya and C. Baggiani *Anal . Bioanal. Chem.,* 2014, **20***,* 4841-4849.
32. M. Yusuf, F.M. Elfghi, S. Abbas Zaidi, E.C. Abdullahab and M. Ali Khan, *RSC Adv.,* 2015, **5**, 50392–50420.
33. G. Williams, B. Seger and P.V. Kamat, *ACS Nano*, 2008, **2**, 1487–1491.